Published in final edited form as:
Molinari, V., Clavel, G., Graglia, M., Antonietti, M., & Esposito, D. (2016). Mild Continuous Hydrogenolysis of Kraft Lignin over Titanium Nitride-Nickel Catalyst. *ACS Catalysis, 6*(3), 1663-1670. doi:10.1021/acscatal.5b01926.

Mild Continuous Hydrogenolysis of Kraft Lignin over Titanium Nitride-Nickel Catalyst

Abstract

Lignin is one of the most important candidates for the procurement of renewable aromatics. The development of successful strategies for the production of building blocks from lignin implies the design of effective depolymerization protocols. Here we propose a continuous flow approach for the hydrogenolysis of Kraft lignin utilizing a TiN-Ni heterogeneous catalyst. The refining of commercial Kraft lignin was evaluated, showing that the catalyst can facilitate the partial depolymerization of this sulfur-containing material under very mild conditions and with short residence times. The process restitutes lignin in the form of oligomers in combination with an array of valuable single-ring aromatic compounds.

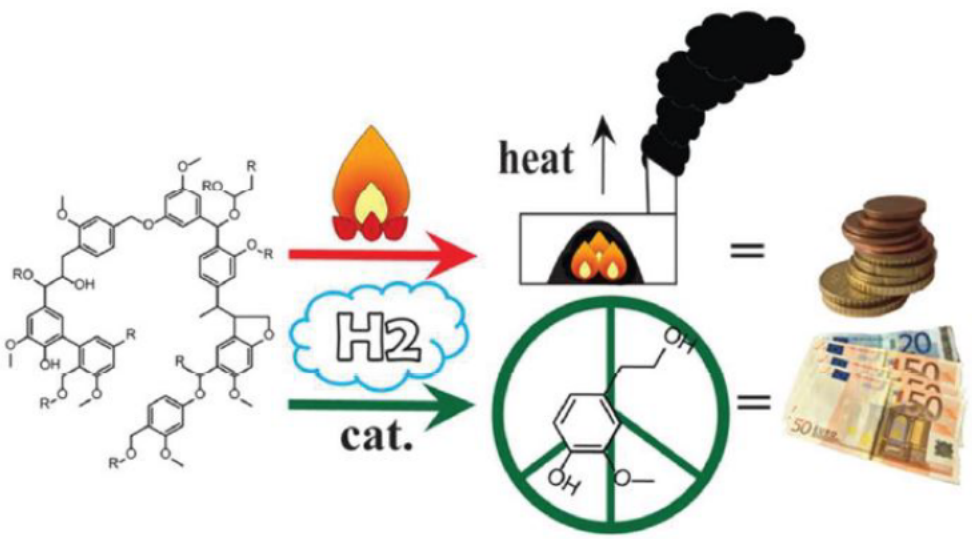

Mild Continuous Hydrogenolysis of Kraft Lignin over Titanium Nitride-Nickel Catalyst

*Valerio Molinari, Guylhaine Clavel, Micaela Graglia, Markus Antonietti and Davide Esposito**

Author Address: Max-Planck-Institute of Colloids and Interfaces, 14424 Potsdam, Germany.

Abstract: Lignin is one of the most important candidates for the procurement of renewable aromatics. The development of successful strategies for the production of building blocks from lignin implies the design of effective depolymerisation protocols. Here we propose a continuous flow approach for the hydrogenolysis of kraft lignin utilizing a TiN-Ni heterogeneous catalyst. The refining of commercial kraft lignin was evaluated, showing that the catalyst can facilitate the partial depolymerisation of this sulfur containing material under very mild conditions and short residence times. The process restitutes lignin in the form of oligomers in combination with an array of valuable single-ring aromatic compounds.

Keywords: Lignin, Heterogeneous catalysis, Titanium Nitride, Nickel, Hydrogenation.

Introduction: The paper industry produces millions of tons of lignin every year (50 million in 2004)[1], which is mainly employed for the production of heat energy.[2-4] However, such raw material has a high potential to be valorized, being among the most important candidates to replace fossil feedstock for the production of aromatic molecules.[5,6] Industrial production of aromatics from lignin relies on the development of robust deconstruction (depolymerisation) technology. Recently, research on lignin depolymerisation is intensifying despite the

challenges. The structure of lignin is extremely heterogeneous and strongly depends on the type of plant (hardwood, softwood etc.) as well as the process used for its extraction,[7-10] making literature comparison not easy.[1] Among the proposed strategies, the use of catalytic hydrogenolysis has received strong attention. According to recently published works, lignin depolymerisation by aryl ether cleavage requires generally high temperatures (170–320 °C) as well as long reaction times (8–12 hours) for hydrogenation with H_2[11-28]. On the other hand, milder conditions were achieved via transfer hydrogenation process (120–195 °C, 1-8 hours). Nevertheless, the search for the ideal catalyst is still ongoing,[15,24,28-35] with Ni-based systems being the foremost candidates. In this regard, new synthesis routes and metal supports are being evaluated to improve the activity of Ni-based catalysts as well as their tolerance towards sulfur introduced in the lignin structure during specific pulping processes. We recently introduced a new nanocomposite catalyst based on nickel and titanium nitride (TiN-Ni),[36] inspired by the concept that metal nitrides and carbides can modulate the properties of neighboring nanoparticles due to favorable electronic interactions.[37-39] TiN-Ni was found to be efficient for the hydrogenolysis of model molecules representing three of the most abundant ether bonds (α-O-4, β-O-4 and 4-O-5) found in the lignin structure, exhibiting its promise as a new candidate for lignin refinery. In our previous report we observed a superior activity for TiN-Ni compared to Ni on carbon, suggesting an influence of the TiN electronic structure on the supported Ni. In this contribution we investigated important structural features of this novel system, and demonstrated that the combination of TiN and Ni works particularly well even if compared to another known catalyst for hydrogenation reactions, such as TiO_2-Ni.[40-43] A TiO_2-Ni system with similar physical characteristics to TiN-Ni was synthesized in order to investigate the specific influence of TiN on the catalytic activity of the composite towards the cleavage of α-O-4 model molecules. In our previous work we also anticipated the conversion of real lignin using TiN-Ni. Here, we fully investigated the hydrogenolysis of commercial kraft lignin, using for the first time a continuous flow system.

The reaction catalysed by the TiN-Ni composite results in the depolymerisation of the macromolecule into a pool of aromatic oligomers and monomers, which can be fractionated by chromatographic methods.

Results and discussion:

Synthesis and characterization of TiX-Ni (X = N, O_2)

TiN-Ni:

Titanium nitride was prepared via the urea route,[44] i.e. through carbothermal reduction of a Ti-urea gel. The addition of Ni on TiN was performed in a second step to obtain the final TiN-Ni composite.[36] Interestingly, X-ray diffraction (XRD) studies showed a shift of the peaks to higher angles in the diffraction pattern of TiN, suggesting a doping effect of Ni on TiN. Therefore, we monitored the shift as a function of the amount of Ni in the composite. Different samples of TiN-Ni with increasing Ni content (molar ratios of 1%, 5%, 10%, 20%, 50%) were prepared (Figures S1 and S2). The diffractogram (Figure 1A) of TiN-Ni with low Ni content (1 mol%) shows a shift in the reflections of TiN (corresponding to a change of cell parameter of Δa ~0.021 Å, Table S1) to higher 2θ values without formation of a Ni phase. The low amount of Ni added in this case is probably introduced entirely into the TiN crystalline structure, decreasing the cell size as a result of the smaller size of Ni compared to Ti atoms, and causing the shift. By increasing the amount of Ni to 10 mol % the formation of the cubic Ni phase is observed at around $2\theta = 44$, accompanied by a progressive broadening of the TiN diffraction signals, which suggests a loss of crystallinity for TiN. The higher amount of Ni inserted into the TiN phase is also responsible for an increase in the magnitude of the shift (Δa ~0.024), as shown in figure 1 A for the (200) plane. Figure S1 additionally shows the shift by comparing the (200) plane of TiN with the (111) of metallic nickel. Interestingly, the corresponding cell shrinkage was also observed for the other planes of the TiN phase (Table S2).

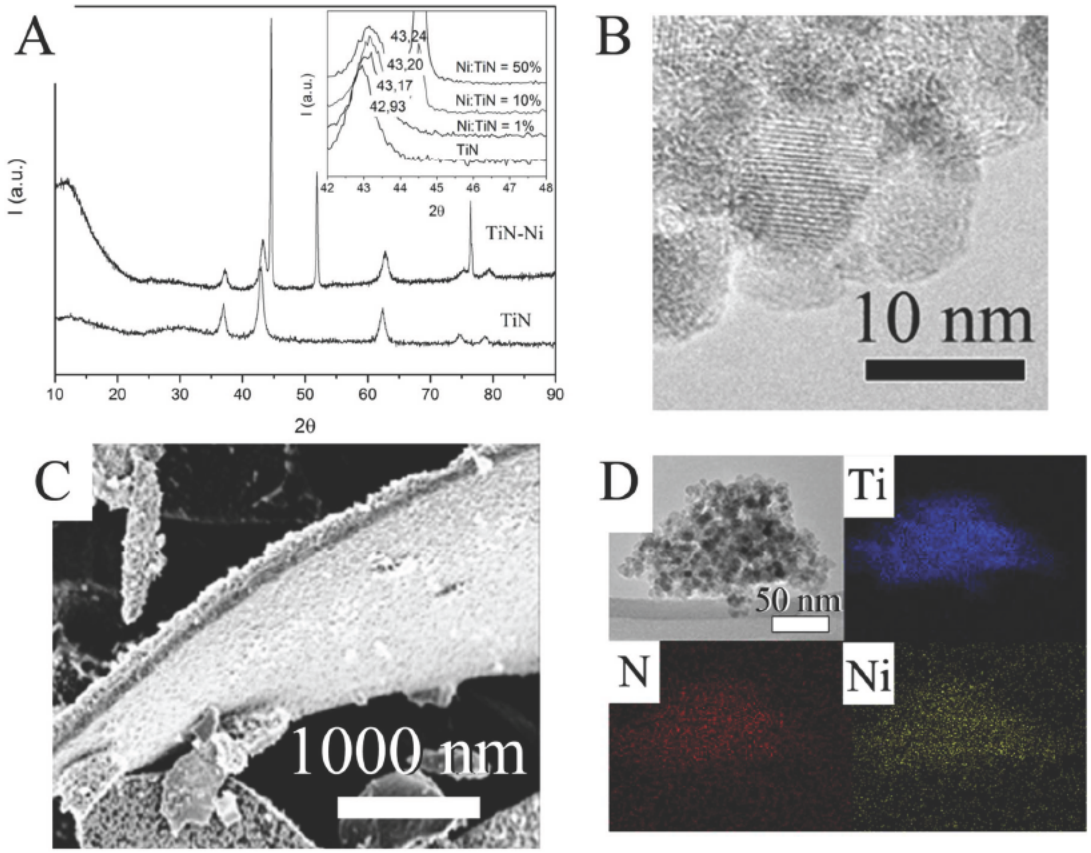

Figure 1: X-ray diffractograms of TiN and TiN-Ni samples (50% molar ratio), the insert shows an enlargement of the (200) diffraction peak of TiN and TiN-Ni (1%, 10% and 50% Ni/Ti molar ratio) (A); HR-TEM of TiN-Ni (50% molar ratio) (B); SEM of TiN-Ni (50%) (C) EDX mapping of TiN-Ni (1 mol%) (D).

The magnitude of the shift remains constant for amounts of Ni >20 mol% (Table S1), revealing that TiN accommodates a maximum amount of Ni in its cell, while the excess forms cubic Ni. Although we initially excluded that the peak shift is caused by the oxidation of TiN, the partial oxidation of the TiN into oxynitride (TiO_xN_y) during the second pyrolysis step by means of oxygen contained in nickel acetate is still possible. To exclude this hypothesis, nickel acetate was systematically replaced with acetic acid in ethanol, sodium acetate and ammonium acetate respectively for the impregnation of TiN followed by thermal treatment (800 °C). In all cases, no evident changes in the final XRD were observed (Figure S3),

supporting the hypothesis that the shift of the peak to wider angles in the TiN-Ni is caused solely by the insertion of Ni. Consistently, the N/O ratio as a function of different Ni loading also exhibited no changes for the different TiN-Ni composites, as estimated by elemental analysis (Table S3). Atomic mapping measurements were performed to verify the distribution of Ni for the low Ni (1%) loaded sample. These experiments revealed that Ni (Figure 1D) is homogeneously distributed in the TiN phase, rather than being localized as nanoparticles/aggregates commonly observed on supported metals, corroborating the doping hypothesis.

As mentioned above, the electronic environment of titanium in the composite can influence the final activity of the catalyst. For instance, previous reports described the change in chemisorption properties of Ni once the metal is supported on TiO_2.[45] According to these studies, Ni can displace oxygen on the surface of TiO_2,[46] formally causing the partial reduction of Ti(IV) to Ti_2O_3. As a result, the corresponding electron-deficient Nickel was less active towards hydrogen uptake[47] and thus its catalytic activity towards hydrogenation reaction was altered. Similar effects have been described previously in the context of metal/semiconductor heterojunctions.[48] We surmised that the different electronic configuration of TiN, in which Ti(III) is more reduced, can modulate this effect resulting in the formation of more reactive Ni sites. While the in-depth elucidation of the composite´s surface properties will be the subject of further studies, we speculate that the different characteristics of Ti in Ti(III)N and Ti(IV)O_2 may result in a different catalytic activity of the TiX-Ni composite. In order to verify this hypothesis we compared TiN-Ni to a novel TiO_2-Ni system with similar features (particle size and surface area) as described in the following section.

TiO_2-Ni:

To allow an efficient comparison between the two materials, a urea route was designed to synthesize TiO_2 nanoparticles inspired by the method employed for the preparation of TiN. The thermal treatment (500 °C) of a Ti-urea gel in air afforded anatase TiO_2 with surface area and particle sizes similar to one of the TiN materials synthesized *via* the urea route (Figure 1B and Figure 2C). Similar synthetic procedures are used in the literature for the production of N-doped TiO_2[49-51]. In our case, the calcination (air atmosphere) of the Ti-urea gel resulted in a material with a nitrogen content of ca. 0.6 % (w/w) (Table S3). The successive addition of Ni was performed using the same procedure followed for TiN-Ni. Interestingly, in this case no obvious peak shift in the diffractogram could be detected (Figure 2A), suggesting that the doping of the Ti phase does not occur in the TiO_2-Ni system. Despite the similar surface area, the final dispersion and size distribution of the Ni particles was different in the two TiX-Ni composites (Table 1, Figure S4 and S5). In particular, TiN resulted in the more efficient stabilization of smaller Ni particles. A comparison of some structural features of TiX and TiX-Ni systems can be found in Table 1.

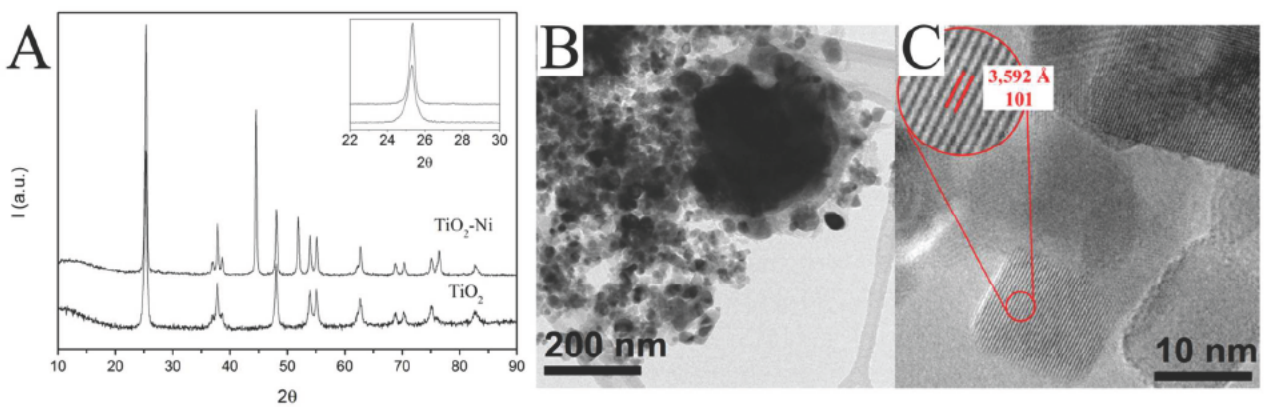

Figure 2: diffractogram of TiO_2 (anatase) and TiO_2-Ni (50 mol%) (A); TEM overview of TiO_2-Ni (50 mol% ratio) (B) and HR-TEM of TiO_2 nanoparticles(C).

Catalytic activity of TiX-Ni composites (X = N, O_2)

Table 1: surface area and average particle/crystallite size of TiX and TiX-Ni materials.

Sample	Surface area (m^2g^{-1})	Average particle/crystallite size of TiN or TiO_2 (nm)		Average particle/crystallite size of Ni (nm)	
		TEM	XRD	SEM	XRD
TiN	212	12	10	-	-
TiN-Ni	117	11	10	61±22	35
TiO_2	230	13	11	-	-
TiO_2-Ni	110	13	11	117±76	36

The aromatic units in the lignin structure are connected by different kinds of bonds (mainly C-O-C and C-C). Among the different aryl ethers, the β-O-4 linkage represents the most abundant bond (45–50%) in lignin, followed by the α-O-4 (6–8%) and 4-O-5 (4–8%).[52] We have previously demonstrated the high efficiency of TiN-Ni for the hydrogenolysis of molecules containing all three kinds of bond. Here, the efficiency of the different TiX-Ni materials for the hydrogenolysis of benzyl phenyl ether (as a model for the α-O-4 linkage) was compared to gain additional insight into the effect of the chemical environment of Ti on the performance of the cleavage. Benzyl phenyl ether was chosen due to the ease of cleavage (compared to β-O-4 and 4-O-5 models) in order to better appreciate the different activities of the catalysts. The screening (Figure 3) proved TiN-Ni as the most active catalyst, although the difference in the catalytic activity is more pronounced in the medium temperature range (100-130 °C) and similar conversions can be achieved with TiO_2-Ni above 140 °C.

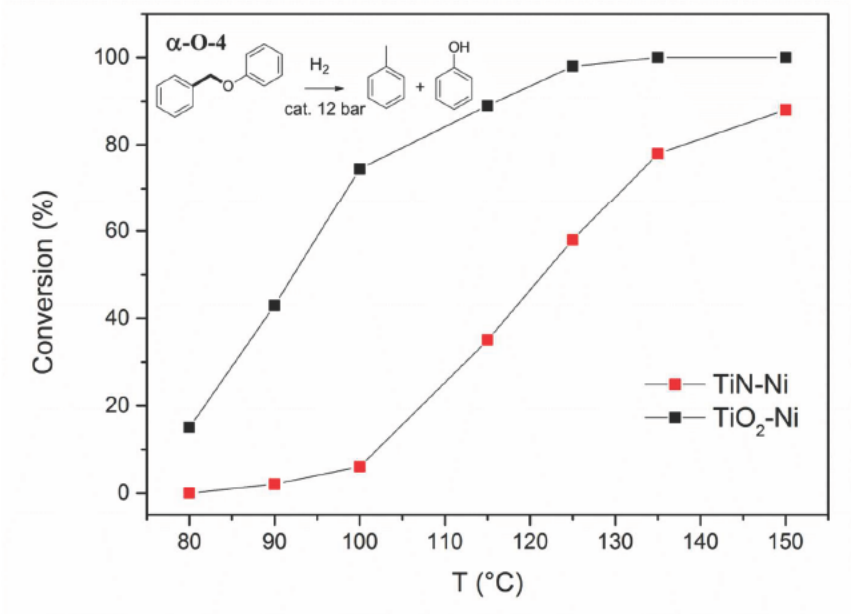

Figure 3: catalytic conversion of benzyl phenyl ether (0.05 M, ethanol) using different TiX-Ni (Ni/Ti = 50 mol%, ~6 mmol of Ni) catalysts. Reaction conditions: 0.5 mL min^{-1} (retention time ~1.8 min), 12 bar.

The TiN-Ni composite catalyzes the quantitative cleavage of benzyl phenyl ether into phenol and toluene (~ 1:1 ratio) in a flow system already at 125°C. In contrast, TiO_2-Ni resulted in a conversion of ~60% at this temperature, with a productivity (defined as P = $mmol_{product}\ g^{-1}_{catalyst}\ h^{-1}$) of 0.7, roughly half of the value compared to that of TiN-Ni (P = 1.3). The difference in productivity is increased at lower temperatures (i.e. $P_{TiN\text{-}Ni}/P_{TiO2}$-Ni ratio is higher than 2 at 115°C), possibly due to an induction period in the case of the TiO_2-Ni catalyzed reaction. The difference in performance between TiN-Ni and TiO_2-Ni can be attributed to two synergistic effects. Firstly, variations in the oxidation state of Ti (in this case from III to IV in TiO_x) have been related in the past to an alteration in H_2 chemisorption properties of the corresponding supported Ni nanoparticle in TiO_x-Ni composites.[47] Therefore, the use of a stable Ti(III) species can have a positive effect on the catalysis, promoting the formation of more reactive Ni sites. Moreover, the nature of the support plays a role in the metal dispersion, thereby effecting the particle size distribution. On the basis of

these considerations we speculate that the urea-derived TiN in combination with Ni performs as an excellent catalyst through a combination of electronic and dispersion effects. Interestingly, the titanium supports of both TiO_2-Ni and TiN-Ni feature similar particle sizes and surface areas, although TiN triggers the formation of smaller Ni nanoparticles. As detected by SEM analysis, TiN is organized in "sheet" structures (Figure 1C), upon which Ni is dispersed on the surface as nanoparticles of ~60 nm average size (Table 1, Figure S4). In the TiO_2-based sample, on the other hand, Ni grows in the form of bigger particles of ~120 nm (Table 1, Figure S5). This fact is in agreement with the observation that, unlike the case of TiN, Ni does not penetrate the lattice of TiO_2 and appears in this case to be less well-dispersed.

The catalytic test on the model molecule revealed that TiN-Ni has a high activity towards ether hydrogenolysis, and thus it was tested for commercial kraft lignin hydrogenolysis.

Hydrogenolysis of Kraft lignin:

In order to implement lignin refinery at a commercial level, the ideal hydrogenolysis process is required to be compatible with the current wood processing technology. Therefore, in this work we targeted lignin produced from the Kraft-process, which is one of the most available sources of lignin and is produced worldwide as a by-product of the paper industry. The average molecular weight of the commercial Kraft lignin used in this study is ~4500 g mol^{-1} (further info in Table S4), as detected by size exclusion chromatography. Interestingly, this form of lignin also features considerable amounts of sulfur (~1.8 wt% by elemental analysis) introduced during pulping in the form of aliphatic thiols. The presence of sulfur, a known poison for metal catalysts,[53-56] is a considerable problem for catalytic processes and for this reason many biorefinery studies have been focusing on alternative sulfur-free lignin preparations (i.e. organosolv lignin).[14,26,57,58] On the other hand, the depolymerisation of Kraft Lignin is to be preferred due to its wide availability. Therefore Kraft Lignin was tested to evaluate the catalytic performance of TiN-Ni, which was additionally compared to that of

TiO_2-Ni and other catalysts previously employed for lignin refinery, including Raney Nickel (RaNi) and Pd/C.[11,16,23,25,27,59,60] A fixed bed reactor acts as a convenient setup to perform hydrogenolysis offering an effective method of separating the reacted lignin from the catalyst and to limit the contact time between the catalyst and the poisonous sulfur species contained within Lignin. On the other hand, flow systems are sensitive to precipitates and deposits that could cause blockages and the solubility of reactants and products throughout the whole process play a key role.

Commercial Kraft lignin (see Table S5) has limited solubility in many common organic solvents with a maximum of ~1.4 mg mL^{-1} in methanol (MeOH), tetrahydrofuran (THF) and dioxane. Since alcohols are effective solvents for hydrogenations, we performed our reactions in methanol. In a scaled up process the solubility of lignin can be enhanced by pre-heating the solution before the reaction in order to increase the productivity of the process and diminish the waste solvent. This possibility is not feasible in our setup; therefore we worked at the maximum lignin concentration (1.4 mg mL^{-1}) at room temperature. In the continuous reactor, the feed solution containing lignin was mixed with hydrogen and then flowed through a catalyst bed (~1 g) at different temperatures and flow rates. In order to quantify the conversion of the reaction, a 100 mL aliquot of the reacted solution was dried in order to estimate its dry content, and then purified by silica column chromatography. In general, three different fractions were isolated employing different mobile phases of increasing polarity (Figures 4 and 5). Each fraction revealed the presence of lignin fragments with a different average molecular weight (Figure 5) depending on the reaction conditions, as summarized in Table 2.

Table 2: Isolated yields of the three fractions derived from lignin hydrogenolysis using different catalysts, retention times, temperatures and solvents.

Entry 1	Reaction conditions			Fraction yield (wt%)		Tot yield (wt%)	Fraction average molecular weight (g mol^{-1})		
	Time (min)	Flow rate (mL min^{-1})	Solvent	1	2		1	2	3
1	-		-	-	-	-	-	-	4467
2	4.5	0.2	MeOH	23.2	39.2	63	647	1908	2834
3	3.0	0.3	MeOH	21.6	40.0	62	682	1745	2511
4	2.3	0.4	MeOH	14.4	49.2	63	720	2157	-
5	1.8	0.5	MeOH	14.2	39.4	54	606	1813	-
6	1.5	0.6	MeOH	17.7	30.8	49	737	1982	-
7[a]	3.0	0.3	MeOH	7.5	20.6	28	650	1652	-
8	3.0	0.3	EtOH	20.0	51.1	71	711	1988	-
9	3.0	0.3	THF	21.6	48.3	70	689	2014	-
10	3.0	0.3	iPrOH	18.4	45.5	64	652	1847	-
11[b]	4.5	0.2	MeOH	32.3	25.7	58	749	1722	3475
12[b]	3.0	0.3	MeOH	30.8	29.2	60	788	1654	-
13 [c]	3.0	0.3	MeOH	12.2	20.3	32.5	602	1480	-
14 [d]	3.0	0.3	MeOH	18.0	25.4	43.4	630	1224	-

Reaction conditions: 150°C, TiN-Ni (50% molar ratio) (~6 mmol of Ni), 25 bar; [a]: 135°C; [b]: RaNi; [c]: Pd/C; [d]: TiO_2-Ni.

Fraction 1, 2 and 3 are obtained from the crude mixture of the reaction by chromatographic purification (see supporting information for further details). The fraction yields were determined on weight percentage (mass of the fraction divided by the mass of the dry content) after silica chromatography.

Reactions with TiN-Ni afforded ca. 140 mg of crude product per 100 mL of eluate. Fraction 1 contained a pool of low molecular weight compounds (<1000 g mol^{-1}), otherwise absent in the lignin starting material. The yield of this fraction was optimized up to 23 wt.% of the dry content at 150 °C and a retention time of ~4.5 minutes (Table 2, entry 2), the harshest conditions achievable using our non-customized reactor. In principle, the yield of fraction 1 can be enhanced by performing the reaction at higher temperatures and longer retention times.[12,15,17-19,61,62] The yield of the second fraction, isolated in ~40 wt. %, presents a higher average molecular weight (~1000–2000 g mol^{-1}) and consists of molecules with ~10

interconnected aromatic rings in average. The cumulative yield of fraction 1 and 2 was ~60 wt.% (fraction 3 was considered to be unreacted lignin) at a flow rate of 0.3 mL min^{-1}.

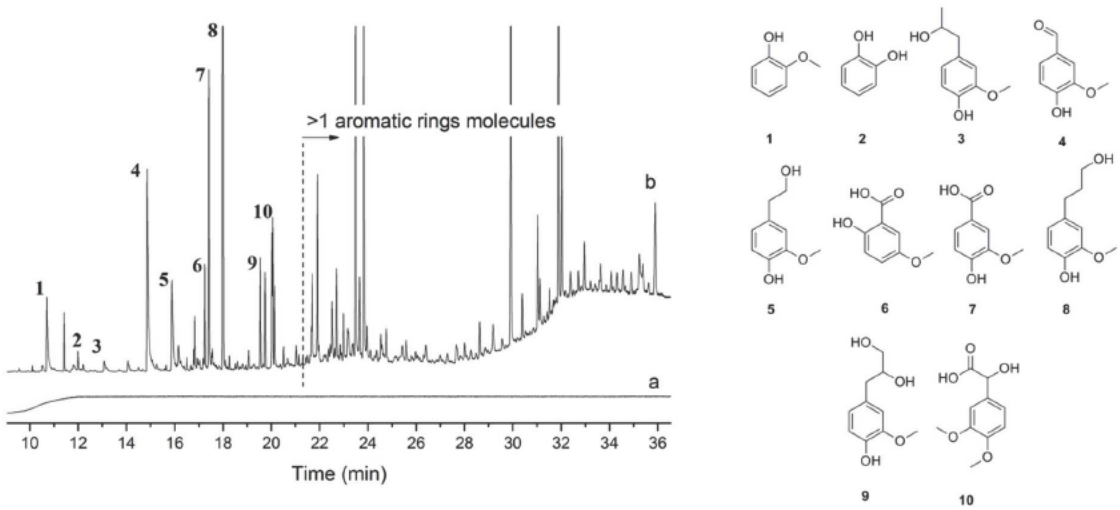

Figure 4: GC-MS of (a) starting lignin and (b) fraction 1 after reaction over TiN-Ni catalyst (Table 2, entry 2).

Interestingly, the 2D HSQC NMR analysis of fraction 1 (Figure S8) suggests the reduction of β-O-4 linkages signals compared to the pristine lignin (Figure S9), providing evidence of an effective depolymerisation. Gas chromatography combined with mass spectroscopy (GC-MS) was utilized for a qualitative analysis of the aromatic monomers contained in fraction 1 (Figure 4). The chromatogram shows the presence of different substituted guaiacol products, together with biaryl units interconnected by C-C bonds. GC-FID was thus used for quantitative analysis. The calibrated total area of the GC chromatogram accounts for 3.2% of fraction 1 (figure S11). The difference between isolated and GC-FID yields can be explained by the presence of GC "silent molecules" (from trimers to hexamers), consistent with GPC data. Performing the reaction using TiO_2-Ni (Table 2, entry 14) resulted in a drop in yield compared to TiN-Ni, although the dry content of the crude product was the same (ca. 140 mg for 100 mL), suggesting a less effective depolymerization. Interestingly, the selectivity of the reaction appeared to be notably altered, as shown in Figure S11, with a reduced formation of

guaiacol and catechol among others compounds. At this stage, we compared these results with the performance of representative commercially available catalysts which have been proposed for the depolymerization of lignin. Interestingly, using Pd/C as the catalyst, a similar selectivity to the case of TiO_2-Ni was observed (Figure S11). However, the yields appeared to be lower compared to the case of TiN-Ni (table 2, entry 13) and associated with a lower dry content in the eluate (90 mg in 200 mL).

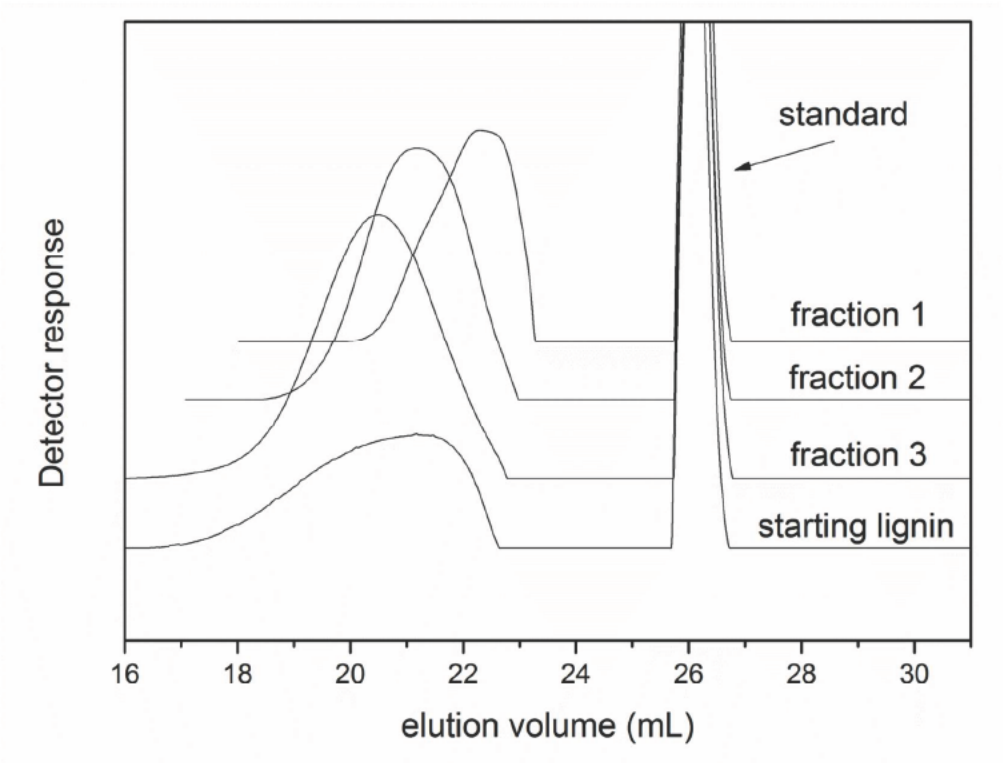

Figure 5: Size exclusion chromatography of starting lignin together with the three isolated fractions after reaction (Table 2, entry 4).

Use of Raney-Ni for the same reaction afforded fractions with similar molecular weight distributions and in comparable yields (entry 12), together with comparable selectivities to those observed for TiN-Ni for the formation of small molecular weight molecules (Figure S12). Nevertheless, in this case, the dry content was found to be slightly reduced pointing to the possible formation of coke on the catalysts or the adsorption of lignin on the solid support.

This prompted an evaluation of the time on stream stability for the different catalysts, as described in the next paragraph.

Stability tests

Evaluation of catalyst stability was performed under "forced conditions" (i.e. conversion < 80%). TiN-Ni appears to be stable under said conditions for up to ca. 500 hours of utilization (~15 grams of lignin with ~1 gram of TiN-Ni) (Figure 6A), with no significant changes in the crystalline phases, nor significant alterations in the crystallite size of TiN and Ni (Figure 6B).

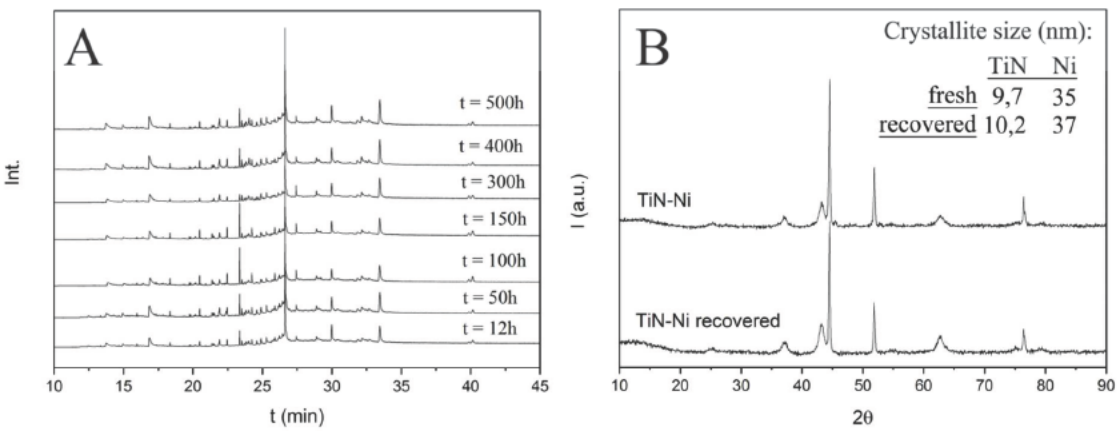

Figure 6: time on stream of Kraft lignin over TiN-Ni (50%) for 500 hours, 0.3 mL min^{-1}, 25 bar, 150 °C (samples injected into the GC-MS without derivatization of the reaction mixture) (A) diffractions of TiN-Ni (50%) fresh and recovered after 500 hours of reaction, with the corresponding crystallite size of the two phases (calculated by the Scherrer equation)(B).

Interestingly, the presence of sulfur species (e.g. nickel sulfide) in the recovered catalyst was excluded by XRD. SEM analysis (Figure S13) in turn showed a slight change in the morphology of the TiN-Ni composite. The sheet macrostructure partially collapsed and a small degree of agglomeration was visible, although distinct non aggregated Ni particles can still be observed on the catalyst surface. In order to better appreciate the possible decrease in activity associated with this morphology change, we monitored the yield of two specific products, namely 2-Methoxy-4-propylphenol and Homovanillyl alcohol, as a function of the

time on stream (Figures S13 and S14). The yields of these two products remain relatively constant over 500 hours, confirming that the catalytic activity does not experience a significant decrease. To further evaluate the stability of the catalyst, we performed an additional test for the hydrogenolysis of benzyl phenyl ether using TiN-Ni batches which have been employed for lignin depolymerisation (Figure 7A) at different times. After 60 hours of exposure to lignin we observed a decrease of catalytic activity compared to the fresh catalyst, until a more stable activity profile is reached. In comparison, TiO_2-Ni exhibited a drastic decrease in catalytic activity after just ~20 hours of lignin exposition. At this stage, the conversion of benzyl phenyl ether dramatically dropped and hit a maximum of ~25% at 150°C (Figure 7B). The reason for the deactivation of TiO_2-Ni could be related to sintering or leaching of Ni particles, however was not investigated at this stage.

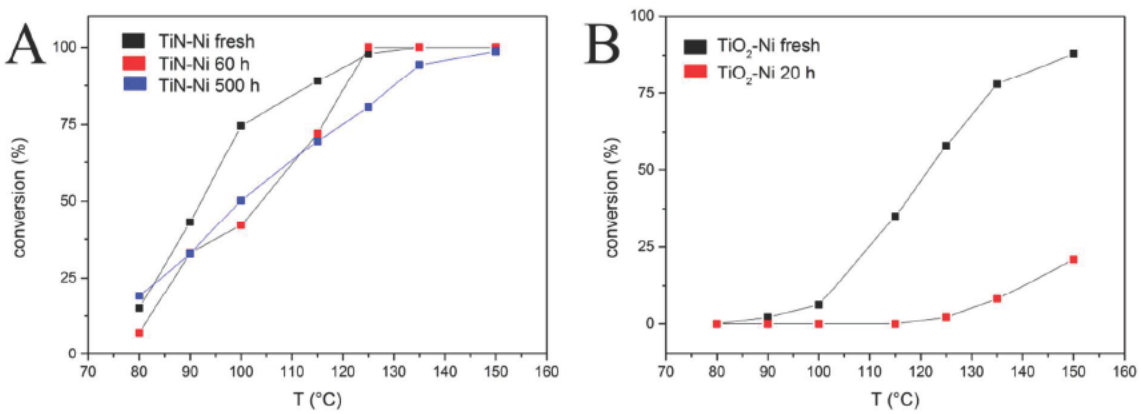

Figure 7: catalytic conversion of benzyl phenyl ether (0.05 M, EtOH) using TiN-Ni (50%, ~6 mmol of Ni (A) and TiO_2-Ni (50%, ~6 mmol of Ni) (B) catalysts, before and after 20, 60 or 500 hours of lignin exposition. Reaction conditions: 0.5 mL min^{-1} (~1.8 min), 12 bar.

Stability tests performed on Pd/C and RaNi during the hydrogenolysis of lignin displayed a very different trend compared to TiN-Ni. In particular, the reaction with Pd/C experienced a considerable pressure drop after 12 hours on stream, leading eventually to a system blockage, which hampered the further evaluation of the stability. High surface area carbon materials are often characterized by microporous structures that result in a high tendency to adsorb

reactants, and are reported to be sensitive to pore blockage by coke deposits. Such effects, which represent a drawback especially in continuous flow applications, have been recently reported in the case of lignin processing. For instance, experiments on lignin pyrolysis using Iron supported on activated carbon as the catalyst resulted in severe blockage of the microporous system accompanied by catalyst deactivation. [63] For this reason, gas sorption analysis was performed on fresh and used Pd/C powders. The comparison of the nitrogen sorption experiments showed drastic differences (Figure S16). The specific surface area decreased from ~960 $m^2 g^{-1}$ to 228 $m^2 g^{-1}$ after reaction and a similar trend was observed for the pore volume, decreased from 0,589 mL g^{-1} to 0,185 mL g^{-1}, suggesting pores blockage as the main reason for deactivation and the observed pressure drop. Raney Nickel exhibited a similar behavior as Pd/C, although lignin hydrogenolysis could be performed up to 60 hours (Figure S17). Also in this case, a pressure drop resulted in the blockage of the reactor accompanied by leakage of small amounts of a powdered solid from the catalyst bed. Interestingly, XRD and IR analysis of this powder by-product revealed the presence of species that could be related to Nickel hydroxide and Nickel sulfate hexahydrate (Figure S18). However, considering the pyrophoric nature of Raney-Ni, we did not perform in depth analysis on the spent catalyst. In general, the TiN-Ni exhibited a superior stability during lignin hydrogenolysis, compared to TiO_2-Ni. In addition, unlike Pd/C and Raney Ni, TiN-Ni was not subjected to detectable catalyst fouling over 500 hours on stream. This positive effect could be attributed to the specific porosity of TiN-Ni[36] that features a relatively lower amount of micropores compared to Pd/C and will be evaluated in depth in future studies. Finally, the sulfur present in the lignin also appeared to be well tolerated by the TiN-Ni composite, within the limit of the experimental conditions evaluated in the present study. The possibility of performing reactions under mild conditions with good yields, together with its sulfur resistance make the TiN-Ni material a good candidate for new lignin depolymerisation strategies.

Conclusions

In this work the effect of two different TiX (X= N, O_2) materials on the catalytic activity of the corresponding TiX-Ni composites have been compared. In particular, the catalytic activity of the novel TiN-Ni was compared to TiO_2-Ni, revealing TiN-Ni as the most active catalyst for the hydrogenolysis of benzyl phenyl ether. Titanium oxide was prepared via the urea route following a similar synthetic strategy as in the case of TiN, resulting in a final TiO_2-Ni with similar physical properties to TiN-Ni. The better catalytic performance of TiN-Ni may be due to the better dispersion of Ni in the TiN phase as well as the different oxidation state of Ti (III) compared to the titanium dioxide (IV), which is known to alter the behavior of the material towards hydrogen uptake. TiN-Ni exhibited high activity for the hydrogenolysis of kraft lignin, one of the most available types of lignin, yet the most difficult to upgrade via catalytic processes due to the presence of sulfur in its structure. The depolymerisation of this macromolecule yielded the formation of substituted phenols (3.2 wt%) together with many aromatic fragments of smaller molecular weight (up to ~60 wt%) compared to pristine lignin. It can be speculated that the amount of phenols produced can be improved at higher temperatures and longer retention time. TiN-Ni displayed a superior activity compared to TiO_2-Ni. In addition, although similar yields could be obtained employing other known catalysts for lignin hydrogenolysis, such as Raney Ni and Pd/C, the stability of TiN-Ni appeared to be superior and a lower tendency to deactivation was observed compared to Pd/C or Raney Ni. In particular, fouling and lignin adsorption on the catalysts, which resulted in the rapid deactivation of Pd/C or Raney Ni, were not pronounced in the case of TiN-Ni.

Crucially, this work is one of the first reports on the use of a continuous system for lignin depolymerisation and represents a new opportunity for lignin refinery. Future studies will focus on a deeper investigation into catalyst stability and the role of the electronic configuration of TiN on the catalytic activity of TiN-Ni, as well as on the possible scale-up of the process.

Acknowledgements

The authors thank the Max Planck-Fraunhofer cooperation scheme for financial support and the Fritz Haber institute for TEM support.

Supporting Information.

Experimental details, and further characterization of the materials, are available in the Supporting Information. This material is available free of charge via the Internet at http://pubs.acs.org.

Corresponding Author

*Davide Esposito, davide.esposito@mpikg.mpg.de

References

(1) Zakzeski, J.; Bruijnincx, P. C. A.; Jongerius, A. L.; Weckhuysen, B. M. *Chem. Rev.* **2010**, *110*, 3552-3599.
(2) Graglia, M.; Kanna, N.; Esposito, D. *ChemBioEng Rev.* **2015**, *2*, 377-392.
(3) Lehr, V.; Sarlea, M.; Ott, L.; Vogel, H. *Catal. Today* **2007**, *121*, 121-129.
(4) Bozell, J. In *Selective Catalysis for Renewable Feedstocks and Chemicals*; Nicholas, K. M., Ed.; Springer International Publishing, Switzerland: **2014**; Vol. 353, p 229-255.
(5) Marshall, A.-L.; Alaimo, P. J. *Chem. Eur. J.* **2010**, *16*, 4970-4980.
(6) Amen-Chen, C.; Pakdel, H.; Roy, C. *Bioresour. Technol.* **2001**, *79*, 277-279.
(7) Gosselink, R. J. A.; Abächerli, A.; Semke, H.; Malherbe, R.; Käuper, P.; Nadif, A.; van Dam, J. E. G. *Ind. Crop. Prod.* **2004**, *19*, 271-281.
(8) Wörmeyer, K.; Ingram, T.; Saake, B.; Brunner, G.; Smirnova, I. *Bioresour. Technol.* **2011**, *102*, 4157-4164.
(9) Ingram, T.; Wörmeyer, K.; Lima, J. C. I.; Bockemühl, V.; Antranikian, G.; Brunner, G.; Smirnova, I. *Bioresour. Technol.* **2011**, *102*, 5221-5228.
(10) Perez-Cantu, L.; Schreiber, A.; Schütt, F.; Saake, B.; Kirsch, C.; Smirnova, I. *Bioresour. Technol.* **2013**, *142*, 428-435.
(11) Wang, X.; Rinaldi, R. *Energy Environ. Sci.* **2012**, *5*, 8244-8260.
(12) Galkin, M. V.; Samec, J. S. M. *ChemSusChem* **2014**, *7*, 2154-2158.
(13) Toledano, A.; Serrano, L.; Pineda, A.; Romero, A. A.; Luque, R.; Labidi, J. *Appl. Catal., B* **2014**, *145*, 43-55.
(14) Toledano, A.; Serrano, L.; Balu, A. M.; Luque, R.; Pineda, A.; Labidi, J. *ChemSusChem* **2013**, *6*, 529-536.
(15) Zhang, J.; Asakura, H.; van Rijn, J.; Yang, J.; Duchesne, P.; Zhang, B.; Chen, X.; Zhang, P.; Saeys, M.; Yan, N. *Green Chem.* **2014**, *16*, 2432-2437.
(16) Ferrini, P.; Rinaldi, R. *Angew. Chem. Int. Ed.* **2014**, *53*, 8634-8639.
(17) Zakzeski, J.; Jongerius, A. L.; Bruijnincx, P. C. A.; Weckhuysen, B. M. *ChemSusChem* **2012**, *5*, 1602-1609.
(18) Matson, T. D.; Barta, K.; Iretskii, A. V.; Ford, P. C. *J. Am. Chem. Soc.* **2011**, *133*, 14090-14097.

(19) Barta, K.; Matson, T. D.; Fettig, M. L.; Scott, S. L.; Iretskii, A. V.; Ford, P. C. *Green Chem.* **2010**, *12*, 1640-1647.
(20) Luo, Z.; Wang, Y.; He, M.; Zhao, C. *Green Chem.* **2016**, 18, 433-441.
(21) Kloekhorst, A.; Heeres, H. J. *ACS Sustainable Chemistry & Engineering* **2015**, 1905-1914.
(22) Ye, Y.; Zhang, Y.; Fan, J.; Chang, J. *Bioresour. Technol.* **2012**, *118*, 648-651.
(23) Van den Bosch, S.; Schutyser, W.; Koelewijn, S. F.; Renders, T.; Courtin, C. M.; Sels, B. F. *Chem. Commun.* **2015**, *51*, 13158-13161.
(24) Esposito, D.; Antonietti, M. *Chem. Soc. Rev.* **2015**, *44*, 5821-5835.
(25) Wang, X.; Rinaldi, R. *Angew. Chem. Int. Ed.* **2013**, *52*, 11499-11503.
(26) Wang, X.; Rinaldi, R. *ChemSusChem* **2012**, *5*, 1455-1466.
(27) Xin, J.; Zhang, P.; Wolcott, M. P.; Zhang, X.; Zhang, J. *Bioresour. Technol.* **2014**, *155*, 422-426.
(28) Zaheer, M.; Kempe, R. *ACS Catalysis* **2015**, *5*, 1675-1684.
(29) Sturgeon, M. R.; O'Brien, M. H.; Ciesielski, P. N.; Katahira, R.; Kruger, J. S.; Chmely, S. C.; Hamlin, J.; Lawrence, K.; Hunsinger, G. B.; Foust, T. D.; Baldwin, R. M.; Biddy, M. J.; Beckham, G. T. *Green Chem.* **2014**, *16*, 824-835.
(30) Feghali, E.; Cantat, T. *Chem. Commun.* **2014**, *50*, 862-865.
(31) Zaheer, M.; Hermannsdörfer, J.; Kretschmer, W. P.; Motz, G.; Kempe, R. *ChemCatChem* **2014**, *6*, 91-95.
(32) Song, Q.; Cai, J.; Zhang, J.; Yu, W.; Wang, F.; Xu, J. *Chin. J. Cat.* **2013**, *34*, 651-658.
(33) He, J.; Zhao, C.; Mei, D.; Lercher, J. A. *J. Catal.* **2014**, *309*, 280-290.
(34) He, J.; Zhao, C.; Lercher, J. A. *J. Am. Chem. Soc.* **2012**, *134*, 20768-20775.
(35) Chen, X.; Yan, N. *Catal Surv Asia* **2014**, 1-13.
(36) Molinari, V.; Giordano, C.; Antonietti, M.; Esposito, D. *J. Am. Chem. Soc.* **2014**, *136*, 1758-1761.
(37) Chen, W.-F.; Sasaki, K.; Ma, C.; Frenkel, A. I.; Marinkovic, N.; Muckerman, J. T.; Zhu, Y.; Adzic, R. R. *Angew. Chem. Int. Ed.* **2012**, *51*, 6131-6135.
(38) Ji, N.; Zhang, T.; Zheng, M.; Wang, A.; Wang, H.; Wang, X.; Chen, J. G. *Angew. Chem.* **2008**, *120*, 8638-8641.
(39) Tang, C.; Wang, D.; Wu, Z.; Duan, B. *Int. J. Hydrogen Energy* **2015**, *40*, 3229-3237.
(40) Kumar, V. V.; Naresh, G.; Sudhakar, M.; Tardio, J.; Bhargava, S. K.; Venugopal, A. *Appl. Catal., A* **2015**, *505*, 217-223.
(41) Barrientos, J.; Lualdi, M.; Suárez París, R.; Montes, V.; Boutonnet, M.; Järås, S. *Appl. Catal., A* **2015**, *502*, 276-286.
(42) Prakash, M. G.; Mahalakshmy, R.; Krishnamurthy, K. R.; Viswanathan, B. *Catal. Sci. Technol.* **2015**, *5*, 3313-3321.
(43) Varkolu, M.; Velpula, V.; Pochamoni, R.; Muppala, A.; Burri, D.; Kamaraju, S. *Appl Petrochem Res* **2015**, 1-9.
(44) Giordano, C.; Erpen, C.; Yao, W.; Milke, B.; Antonietti, M. *Chemistry of Materials* **2009**, *21*, 5136-5144.
(45) Tauster, S. J.; Fung, S. C.; Garten, R. L. *J. Am. Chem. Soc.* **1978**, *100*, 170-175.
(46) Chung, Y.-W.; Xiong, G.; Kao, C.-C. *J. Catal.* **1984**, *85*, 237-243.
(47) Tauster, S. J. *Acc. Chem. Res.* **1987**, *20*, 389-394.
(48) Li, X.-H.; Antonietti, M. *Chem. Soc. Rev.* **2013**, *42*, 6593-6604.
(49) Cong, Y.; Zhang, J.; Chen, F.; Anpo, M. *The Journal of Physical Chemistry C* **2007**, *111*, 6976-6982.
(50) Mitoraj, D.; Kisch, H. *Angew. Chem. Int. Ed.* **2008**, *47*, 9975-9978.

(51) Livraghi, S.; Chierotti, M. R.; Giamello, E.; Magnacca, G.; Paganini, M. C.; Cappelletti, G.; Bianchi, C. L. *The Journal of Physical Chemistry C* **2008**, *112*, 17244-17252.
(52) Chakar, F. S.; Ragauskas, A. J. *Ind. Crop. Prod.* **2004**, *20*, 131-141.
(53) Bartholomew, C. H.; Weatherbee, G. D.; Jarvi, G. A. *J. Catal.* **1979**, *60*, 257-269.
(54) Dunleavy, J. K. *Platinum Met. Rev.* **2006**, *50*, 110-110.
(55) Oudar, J. *Catalysis Reviews* **1980**, *22*, 171-195.
(56) Lee, J. Y.; Rao, S. V.; Kumar, B. N.; Kang, D. J.; Reddy, B. R. *J. Hazard. Mater.* **2010**, *176*, 1122-1125.
(57) Pandey, M. P.; Kim, C. S. *Chemical Engineering & Technology* **2011**, *34*, 29-41.
(58) Zhang, J.; Teo, J.; Chen, X.; Asakura, H.; Tanaka, T.; Teramura, K.; Yan, N. *ACS Catalysis* **2014**, *4*, 1574-1583.
(59) Zhao, C.; Lercher, J. A. *ChemCatChem* **2012**, *4*, 64-68.
(60) Galkin, M. V.; Sawadjoon, S.; Rohde, V.; Dawange, M.; Samec, J. S. M. *ChemCatChem* **2014**, *6*, 179-184.
(61) Song, Q.; Wang, F.; Cai, J.; Wang, Y.; Zhang, J.; Yu, W.; Xu, J. *Energy Environ. Sci.* **2013**, *6*, 994-1007.
(62) Jiang, Y. T.; Li, Z.; Tang, X.; Sun, Y.; Zeng, X. H.; Liu, S. J.; Lin, L. *Energy & Fuels* **2015**, *29*, 1662-1668.
(63) Olcese, R. N.; Lardier, G.; Bettahar, M.; Ghanbaja, J.; Fontana, S.; Carré, V.; Aubriet, F.; Petitjean, D.; Dufour, A. *ChemSusChem* **2013**, *6*, 1490-1499.